ADVANCING EARTH AND SPACE SCIENCE

Geophysical Research Letters

RESEARCH LETTER

10.1029/2021GL095003

Key Points:

- High latitude magnetopause reconnection with different northward IMF clock angles is studied by using 3-D global hybrid simulations
- High latitude magnetopause flux ropes (HLMFRs) with four topologies of magnetic field lines are formed by multiple X-line reconnection
- IMF clock angle effects where the HLMFRs occurs and the direction of the HLMFRs' axis

Correspondence to:

S. Lu and Q. Lu,
lusan@ustc.edu.cn;
qmlu@ustc.edu.cn

Citation:

Guo, J., Lu, S., Lu, Q., Lin, Y., Wang, X., Zhang, Q., et al. (2021). Three-dimensional global hybrid simulations of high latitude magnetopause reconnection and flux ropes during the northward IMF. *Geophysical Research Letters*, *48*, e2021GL095003. https://doi.org/10.1029/2021GL095003

Received 29 JUN 2021
Accepted 17 OCT 2021

Three-Dimensional Global Hybrid Simulations of High Latitude Magnetopause Reconnection and Flux Ropes During the Northward IMF

Jin Guo[1,2], San Lu[1,2], Quanming Lu[1,2], Yu Lin[3], Xueyi Wang[3], Qinghe Zhang[4], Zanyang Xing[4], Kai Huang[1,2], Rongsheng Wang[1,2], and Shui Wang[1,2]

[1]CAS Key Lab of Geospace Environment, School of Earth and Space Sciences, University of Science and Technology of China, Hefei, China, [2]CAS Center for Excellence in Comparative Planetology, Hefei, China, [3]Department of Physics, Auburn University, Auburn, AL, USA, [4]Shandong Provincial Key Laboratory of Optical Astronomy and Solar-Terrestrial Environment, Institute of Space Sciences, Shandong University, Weihai, China

Abstract

When the interplanetary magnetic field (IMF) is northward, magnetic reconnection between the IMF and the geomagnetic field can occur at the high latitude magnetopause, which allows energy transfer from the solar wind into Earth's magnetosphere. In this letter, by using three-dimensional global hybrid simulations, we find that during the northward IMF, high latitude magnetic reconnection both poleward and equatorward of the cusp can occur almost simultaneously. High latitude magnetopause flux ropes (HLMFRs) with four topologies of magnetic field lines can be formed by multiple X-line reconnection. At the center of the HLMFRs, there is a decrease in the surrounding magnetic field magnitude (weak core field) and an increase in parallel temperature. When the IMF is purely northward, the HLMFRs are located at the noon-midnight meridian plane. When the IMF has a positive B_y component, the HLMFRs in the northern hemisphere shift duskward.

Plain Language Summary

When the interplanetary magnetic field (IMF) is southward, magnetic reconnection between the IMF and the Earth's magnetic field can occur at the low latitude magnetopause, and flux ropes are formed. However, when the IMF is northward, the reconnection site is at high latitude magnetopause. In many previous studies, the high latitude magnetopause reconnection with the northward IMF was considered as no flux rope is formed. In this letter, we use computer simulations to investigate the high latitude magnetopause reconnection during the northward IMF in different directions. When the IMF is northward, the high latitude magnetopause flux ropes (HLMFRs) with four types of magnetic field lines are formed. At the center of the HLMFRs, there is a decrease in the surrounding magnetic field magnitude, an increase in parallel temperature. Compared with the flux ropes formed during the southward IMF, the HLMFRs are fewer and smaller. When the IMF is purely northward, the HLMFRs are located at the noon-midnight meridian plane; when the IMF rotates to the duskward (but still northward), the HLMFRs in the northern hemisphere shift duskward.

1. Introduction

When the interplanetary magnetic field (IMF) is southward, it can reconnect with the geomagnetic field at the low latitude magnetopause, which enhances global convection in Earth's magnetosphere and triggers explosive energy conversion, for example, the geomagnetic storms and substorms (Burton et al., 1975; Dungey, 1961). Magnetopause reconnection can form flux transfer events (FTEs; Russell & Elphic, 1978), which is an effective mechanism for energy transport in the solar wind-magnetosphere coupling. FTEs are usually interpreted as magnetopause flux ropes with helical magnetic field lines formed by multiple X-line reconnection (Z. F. Guo et al., 2020; J. Guo et al., 2021a; Hasegawa et al., 2010; Lee & Fu, 1985; Øieroset et al., 2016; Tan et al., 2011; Wang et al., 2019).

When the IMF is northward, magnetopause reconnection between the northward IMF and the geomagnetic field can still occur (e.g., Gosling et al., 1991) in both northern and southern hemispheres, tailward of cusp, resulting in the formation of newly closed field lines, which captures the magnetosheath particles (Lavraud et al., 2006; Lin & Wang, 2006; Onsager et al., 2001; Shi et al., 2013; Song & Russell, 1992). Two types of high latitude reconnection can occur at the magnetopause, one is between the IMF and the tailward semi-open lobe field lines (i.e., reconnection poleward of the cusp), and the other is between the IMF and the closed geomagnetic field lines (i.e., reconnection equatorward of the cusp; Lockwood & Moen, 1999; Zhang et al., 2016). Recently, the two types of reconnection have been found to occur simultaneously at high latitude magnetopause by using a three-dimensional (3-D) global magnetohydrodynamic (MHD) simulation (Zhang et al., 2021). The high latitude magnetopause reconnection site remains fixed for a long time under steady IMF conditions (Fuselier et al., 2000). Continuous high latitude magnetopause reconnection causes particle precipitation from the solar wind into Earth's magnetosphere, leading to dayside auroras (Frey et al., 2003; Øieroset et al., 1997).

Many observations indicated that during the northward IMF, high latitude magnetopause reconnection occurs at a single X line and no flux rope is formed (Berchem et al., 2003; Frey et al., 2019; Fuselier et al., 2014; Gosling et al., 1991; Song & Russell, 1992; Zong et al., 2005). However, Hasegawa et al. (2008) observed that high latitude magnetopause reconnection can occur at two X lines and may form an HLMFR between them. This is consistent with the 3-D global magnetohydrodynamic (MHD) simulation in Berchem et al. (1995), which showed the formation of the HLMFRs during a purely northward IMF by examining the magnetic field structures. Grandin et al. (2020) further studied the plasma signatures (e.g., temperature and density) of the HLMFRs during the purely northward IMF by performing a global hybrid simulation. However, the global hybrid simulation in Grandin et al. (2020) was only 2-D (uniformity and infinite length in the dawn-dusk direction), in which the flux ropes were reduced to magnetic islands. 3-D magnetic structures and plasma signatures of HLMFRs can be studied by a 3-D global hybrid simulation. High latitude magnetopause reconnection with a purely northward IMF was simulated using a 3-D global hybrid model (Lin & Wang, 2006), but the focus was on the formation of the low latitude boundary layer and the structure of reconnection was not investigated.

The occurrence of high latitude magnetopause reconnection has been found to be controlled by the B_y component or clock angle of the northward IMF because the high latitude magnetopause can occur more easily where the IMF is almost antiparallel to the magnetospheric field lines (e.g., Gosling et al., 1991; Fuselier et al., 2002; Laitinen et al., 2007; Lockwood & Moen, 1999; Luhmann et al., 1984; Phan et al., 2003). The occurrence of the proton auroral spots, formed by high latitude magnetopause reconnection, is also controlled by the IMF B_y or clock angle. When the IMF B_y is positive (negative), the dayside proton auroral spot occurs at postnoon (prenoon) in the northern hemisphere, and the opposite in the southern hemisphere (Frey et al., 2003). Moreover, it is easy to speculate that the HLMFRs formed by high latitude magnetopause reconnection at multiple X lines are also controlled by the B_y component or clock angle of the northward IMF.

Following the above rationale, in this letter, by using 3-D global hybrid simulations, we study 3-D magnetic structures and plasma signatures of high latitude magnetopause reconnection (both poleward and equatorward of the cusp) and the resultant HLMFRs during the northward IMF with different clock angles or B_y components.

2. Simulation Model

In this letter, a 3-D dayside global-scale hybrid simulation model (Z. F. Guo et al., 2020; Lin & Wang, 2005, 2006) is used to investigate the high latitude magnetopause reconnection and HLMFRs during northward IMF. In hybrid simulations, ions are treated as particles, and electrons are treated as a massless, charge-neutralizing fluid. The simulation results are described in the geocentric solar-magnetospheric (GSM) coordinate, in which the x-axis points from the Earth to the Sun, the z-axis points to the Earth's northern magnetic pole, and the y axis completes the right-handed system. In the simulation, a spherical coordinate system (r, θ, φ) is employed. To avoid the singular coordinate line along the polar axes, a semi-cone polar angle around the positive and negative polar axes is cut out from the domain. While cutting a semicone polar angle around the positive and negative polar axes, the dayside cusps can be retained due to rotate the polar axis to the y-axis (J. Guo et al., 2021b; Lin & Wang, 2006). However, for the presentation, we use the conventional spherical coordinate system in which the polar angle θ is measured from the positive GSM z-axis, and the azimuthal angle φ from the negative GSM y-axis.

The angle between the GSM-z and projection of IMF in the GSM y-z plane is the IMF clock angle α, and the IMF is represented as $\mathbf{B}_0 = \left(B_{x0}, B_{y0}, B_{z0}\right) = \left(0, \sin\alpha, \cos\alpha\right) B_0$. Three cases with different initial parameters

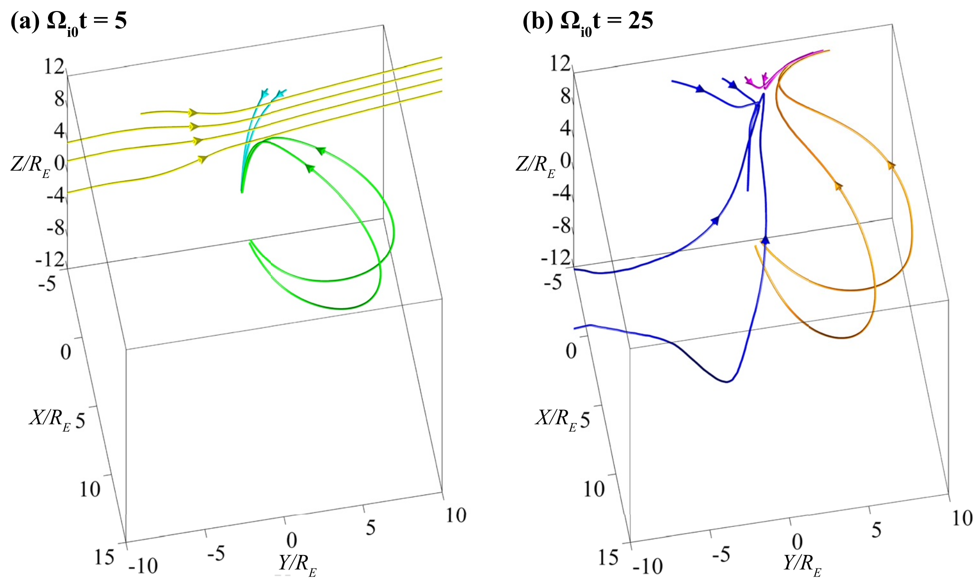

Figure 1. The topological change of field lines during the high latitude magnetopause reconnection obtained from Case 1 at $\Omega_{i0}t$ = 5, and 25. High latitude magnetopause reconnection does not occur at $\Omega_{i0}t$ = 5, but occurs at $\Omega_{i0}t$ = 25. The yellow field lines connected from IMF to IMF; the green field lines connected from MSP to MSP; the blue field lines; the orange field lines connected from MSP to IMF; the cyan field lines are tailward semi-open lobe field lines; the magenta field lines are reconnected free lobe field lines.

are simulated. Case 1 has $\alpha = 80°$, $B_{y0} = 0.9848B_0$, and $B_{z0} = 0.1736B_0$; Case 2 has $\alpha = 40°$, $B_{y0} = 0.6428B_0$, and $B_{z0} = 0.7660B_0$; Case 3 has $\alpha = 0°$, $B_{y0} = 0$, and $B_{z0} = 1B_0$. The simulation domain includes a geocentric distance $3\,R_E \le r \le 27\,R_E$ (where R_E is the Earth's radius), which contains mainly the dayside plasma regions. For these cases with the northward IMF, the simulation domain extends tailward by a 20° (30° in Cases 2 and 3) angle from the y-z plane around the y-axis for both southern and northern hemispheres. The Earth's dipole tilt angle is zero in three cases. A total grid $N_r \times N_\varphi \times N_\theta = 400 \times 200 \times 200$ is used. Nonuniform grids are used in the r direction with a smaller grid size of $\Delta r \approx 0.03\,R_E$ limited to $8\,R_E \le r \le 14\,R_E$. The outflow boundary conditions are utilized at the tailward boundary (the Earth is located at $r = 0$), and solar wind inflow boundary conditions are applied for the outer boundary at $r = 27R_E$. The inner boundary at $r = 3R_E$ is perfectly conducting. The ions are fully kinetic particles besides that the ions in the inner magnetosphere ($r < 7R_E$) are treated as a cold fluid. Initially, the uniform solar wind is placed in $r > 10\,R_E$, and it interacts with the Earth's dipole magnetic field limited to $r \le 10\,R_E$.

A small current-dependent collision frequency (which is current dependent) is used to simulate the anomalous resistivity and trigger magnetic reconnection. The Alfvén Mach number M_A is 5, and the ion and electron plasma beta in the solar wind is set to be $\beta_i = \beta_e = 0.5$. The ion number density in the solar wind is $N_0 = 10000\,R_E^{-3}$. After the simulations begin, the solar wind plasma will flow into the simulation domain along the $-x$-direction. In our simulations, the magnetic field is normalized by the IMF magnitude B_0; the flow velocity is normalized by the solar wind Alfvén speed $V_{A0} = B_0/\sqrt{\mu_0 m_i N_0}$; the time is normalized by $\Omega_{i0}^{-1} = m_i\,/\,eB_0$. A total of $\sim 8 \times 10^8$ particles are used and the time step is $\Delta t = 0.05\Omega_{i0}^{-1}$. The solar wind ion inertial length $d_{i0} = 0.05\,R_E$, which is about three times larger than the realistic value. The global structure of the Earth's magnetosphere is not affected by this kind of scaling (e.g., Omidi et al., 2004; Tóth et al., 2017).

3. Simulation Results

Figure 1 shows the occurrence of high latitude magnetopause reconnection between the IMF and the geomagnetic field in Case 1 (the IMF clock angle is 80°). At $\Omega_{i0}t = 5$, as shown in Figure 1a, the IMF (the yellow field lines) does not reconnect with the geomagnetic field lines (green) or the semi-open lobe field lines (cyan). At $\Omega_{i0}t = 25$, as shown in Figure 1b, two types of high latitude reconnection that can occur at the magnetopause, one is between the IMF (yellow) and the tailward semi-open lobe field lines (cyan), and the other is between the IMF and the closed geomagnetic field lines (green). The former forms the blue semi-open field lines (connected from the IMF to the magnetosphere) and the magenta free field lines, and the latter forms the blue semi-open field lines and the orange semi-open field lines (connected from the magnetosphere to the IMF). These magnetic fields are usually referred to as reconnected magnetic fields.

Figure 2 shows the plasma characteristics and evolution of high latitude magnetopause reconnection in Case 1 (only the reconnection equatorward of the cusp is shown to make the figure easier to understand). The black field lines in Figure 2 represent the reconnected magnetic fields. At $\Omega_{i0}t = 60$ (Figures 2a–2d), high latitude reconnection continues with a decrease in the magnetic field magnitude B_t at the reconnection site (Figures 2a and 2b). The parallel temperature $T_{||}$ slightly increases near the reconnection site (Figure 2c), and bidirectional outflows (mostly in the y-direction, Figure 2d) are formed. At $\Omega_{i0}t = 90$ (Figures 2e–2h), a red flux rope is formed at the center of the reconnection site. The magnetic field magnitude does not increase at the center of the flux rope (Figures 2e and 2f). The parallel temperature is enhanced significantly inside the flux rope (Figure 2g), and the bidirectional reconnection outflows V_y persist (Figure 2h). The length of the flux rope in the axial direction is about $2R_E$ long, and its diameter is about $0.6R_E$. At $\Omega_{i0}t = 115$ (Figures 2i–2l), another small green flux rope appears next to the red flux rope. Similarly, the parallel temperature increases significantly in the green flux rope (Figure 2k). At the same time, the green and red flux ropes are embedded in the reconnection outflow (Figure 2l) and move along with it in the $+y$-direction. At about $\Omega_{i0}t = 120$, the red flux rope disappears because it merges with the piled up reconnected magnetic field (not shown). Note that, in the northern hemisphere, the green and red flux ropes in Case 1 are formed on the duskside of the high latitude magnetopause. This is because in this case with an IMF clock angle 80°, the magnetic shear angle is larger (i.e., the IMF is almost antiparallel to the geomagnetic field) on the duskside, where magnetopause reconnection is more like to occur (Laitinen et al., 2007; Luhmann et al., 1984).

We further examine the field line topologies of the flux ropes. For example, the red flux rope in Figure 2 has four different field line topologies. As shown in Figure 3, the four types of field lines are (a) the blue field line connected from IMF to magnetosphere (MSP), (b) the red field line connected from MSP to IMF, (c) the yellow field line connected from IMF to IMF, and (d) the green field line connected from MSP to MSP. Note that this is similar to the southward IMF case, in which the flux rope formed by multiple X line reconnection between the IMF and the geomagnetic field also has four topologies of magnetic field lines (Lee et al., 1993; Tan et al., 2011). This similarity suggests that the high latitude magnetopause flux ropes (HLMFRs) during the northward IMF are also formed by multiple X-line reconnection.

Figure 4 shows Case 2 with an IMF clock angle of 40°. At $\Omega_{i0}t = 47$, in the northern hemisphere, a flux rope is formed with a decrease in the magnetic field magnitude B_t (Figure 4a) and an increase in parallel temperature $T_{||}$ (Figure 4b) at the high latitude magnetopause. Through the zoom-in views (in the x-y plane) in Figures 4a and 4b, it can be estimated that this flux rope is about $3R_E$ long in the axial direction, and its diameter is about $0.7R_E$. The flux rope is still on the duskside but closer to the noon-midnight meridian plane than the flux ropes are in Case 1. The ion velocity component V_x is shown in Figure 4c, and there are significant reconnection outflows in both the northern and southern hemispheres, as observed by the Cluster spacecraft (Zong et al., 2005). (Note that the contour plane is rotated for 15° around z-axis from the noon-midnight meridian plane.) These reconnection outflows can facilitate the entry of energetic particles from the solar wind into Earth's magnetosphere along the reconnected semi-open field lines.

The results of Case 3 with a purely northward IMF are shown in Figure 5. An HLMFR is formed at $\Omega_{i0}t = 45$, in the northern hemisphere. In this case, the HLMFR is formed by the reconnection poleward of the cusp, because there are no semi-open field lines (connected from magnetosphere to IMF, which only formed by the reconnection equatorward of the cusp) in this HLMFR. Through the zoom-in views (in the x-y plane) in Figures 5a and 5b, it can be estimated that this flux rope is about $3.4R_E$ long in the axial direction, and its diameter is 0.6–$0.9R_E$. Unlike the flux ropes that are on the duskside in Cases 1 and 2, the flux rope in Case 3 is right at the noon-midnight meridian plane. In Case 3, the axial direction of the flux rope is almost along the y-direction, and the reconnection outflows are almost in the x-direction. Note that the high latitude reconnection and HLMFRs occur in the northern and southern hemispheres, but here we only show the northern hemispheric HLMFRs.

10.1029/2021GL095003

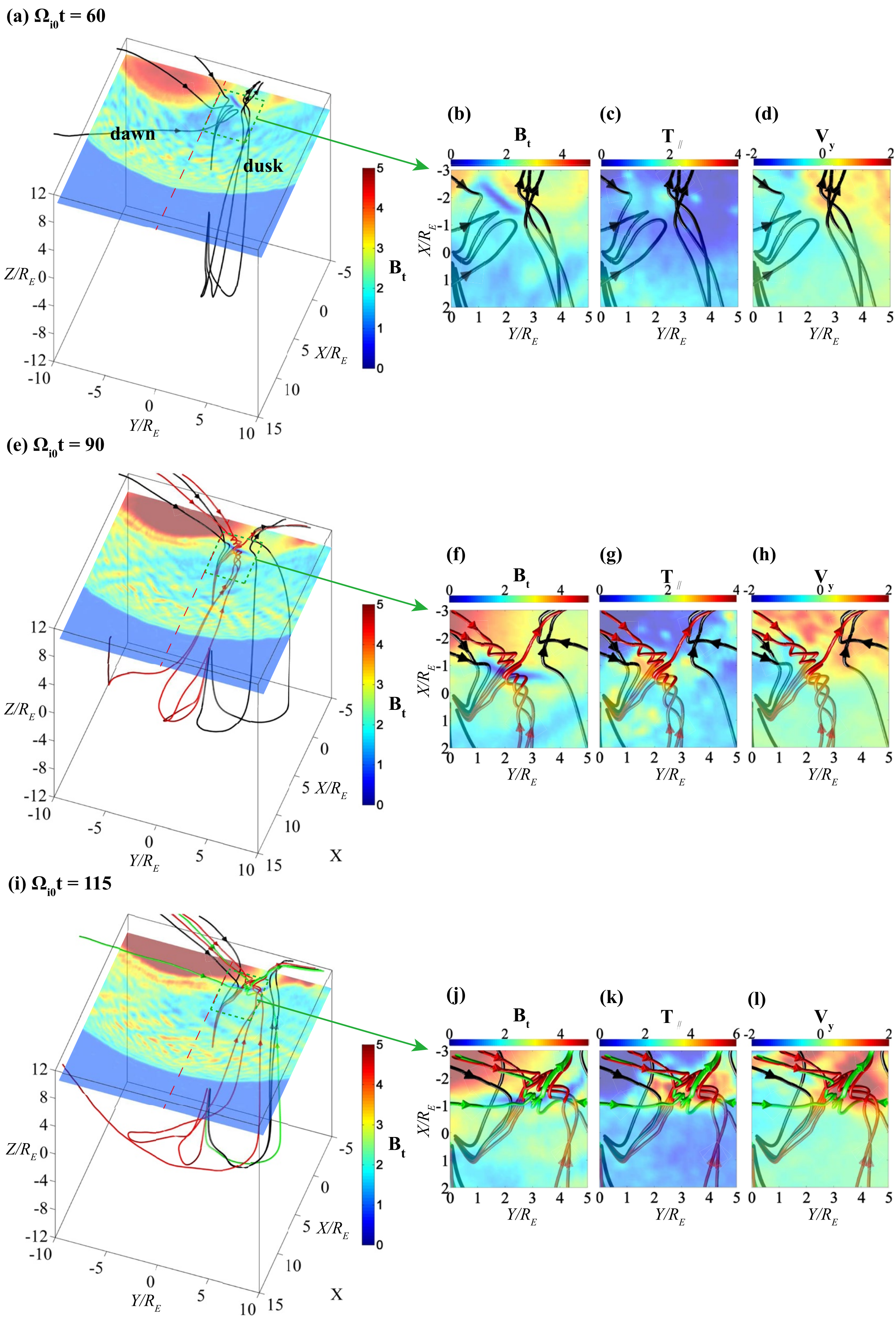

Figure 2.

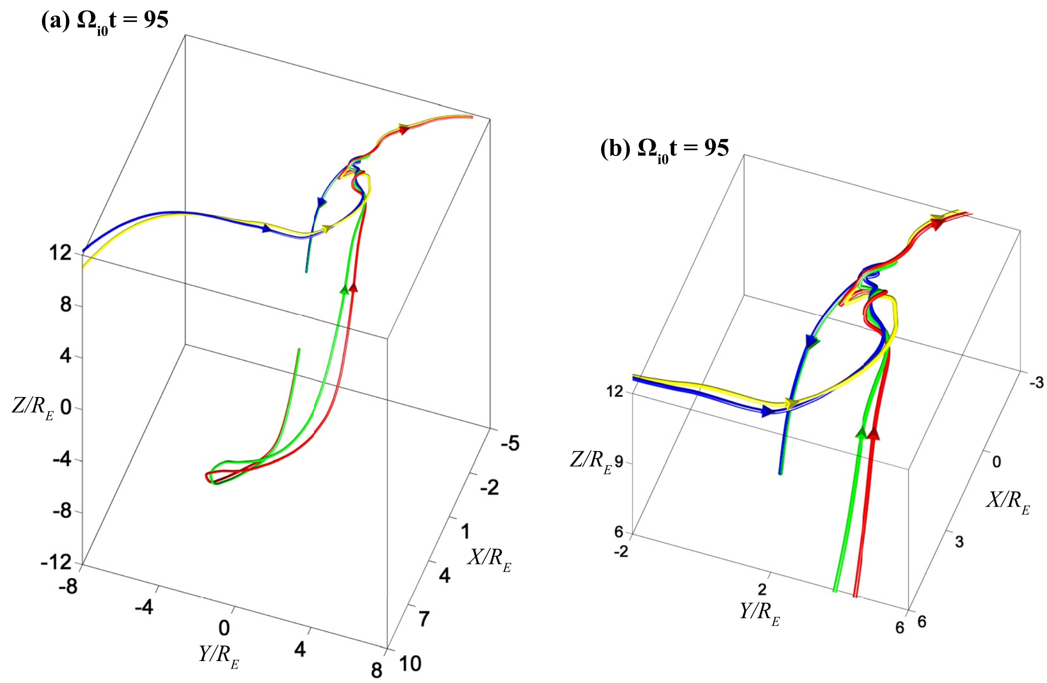

Figure 3. Four field lines of different topologies in the HLMFR obtained from Case 1 at $\Omega_{i0}t = 95$. Here (a) Global view, and (b) Zoom-in view. The blue field line connected from IMF to MSP; the red field line connected from MSP to IMF; the yellow field line connected from IMF to IMF; the green field line connected from MSP to MSP.

4. Conclusions and Discussion

In this study, by using the 3-D global hybrid simulation, we examine the high latitude magnetopause reconnection with different northward IMF clock angles. HLMFRs are formed by multiple X-line reconnection between IMF and geomagnetic field lines in the northern hemisphere. At the reconnection region, significant bidirectional reconnection outflows are formed. Each HLMFR has four topologies of magnetic field lines, which is consistent with the multiple X-line reconnection theory. At the center of the HLMFRs, there is a decrease in the surrounding magnetic field magnitude (weak core field), an increase in parallel temperature. The HLMFRs are smaller than the flux ropes formed at low latitude with the southward IMF. The number of the HLMFRs is also less than that of flux ropes formed with the southward IMF. When IMF B_y is positive (IMF clock angle is 80°), the reconnection site is on the dusk in the northern hemisphere, and the axial direction of HLMFRs is almost along the x-axis. However, when the IMF B_y is zero (IMF clock angle is 0°), the reconnection site is near the noon-midnight meridian plane in the northern hemisphere, and the axial direction of HLMFRs is almost along the y-axis.

Lockwood and Moen (1999) found that there are two types of high latitude reconnection that can occur at the magnetopause, one is between the IMF and the tailward (nightside) semi-open lobe field lines, and the other is between the IMF and the dayside closed geomagnetic field lines. Although our simulation region is primarily on the dayside, it covers a fraction of the nightside cusp, in which the nightside lobe field lines and the reconnection poleward of the cusp can be resolved. Our simulation results of Cases 1 and 2 (with nonzero IMF B_y components) show that the two types of high latitude reconnection occur almost simultaneously, which is consistent with the MHD simulation results in Zhang et al. (2021). However, in Case 3 (without an IMF B_y component), the high latitude reconnection only occurs poleward of the cusp because there are

Figure 2. The plasma characteristics and evolution of high latitude magnetopause reconnection obtained from Case 1 at $\Omega_{i0}t = 60$, 90, and 115. (a), (e), (i) The distribution of magnetic field magnitude B_t in $z = 11R_E$ from a 3-D view, at $\Omega_{i0}t = 60$, 90, and 115. (b)–(d) The distribution of magnetic field magnitude B_t, parallel temperature $T_{\|}$, and ion velocity V_y in the x-y plane ($z = 11R_E$), at $\Omega_{i0}t = 60$. (f)–(h) The distribution of B_t, $T_{\|}$, and V_y in the x-y plane ($z = 11R_E$), at $\Omega_{i0}t = 90$. (j)–(l) The distribution of B_t, $T_{\|}$, and V_y in the x-y plane ($z = 11R_E$), at $\Omega_{i0}t = 115$. The red dotted line represents the position of the noon-midnight meridian plane. The black field lines represent the reconnected magnetic fields; the red and green field lines represent two different flux ropes.

10.1029/2021GL095003

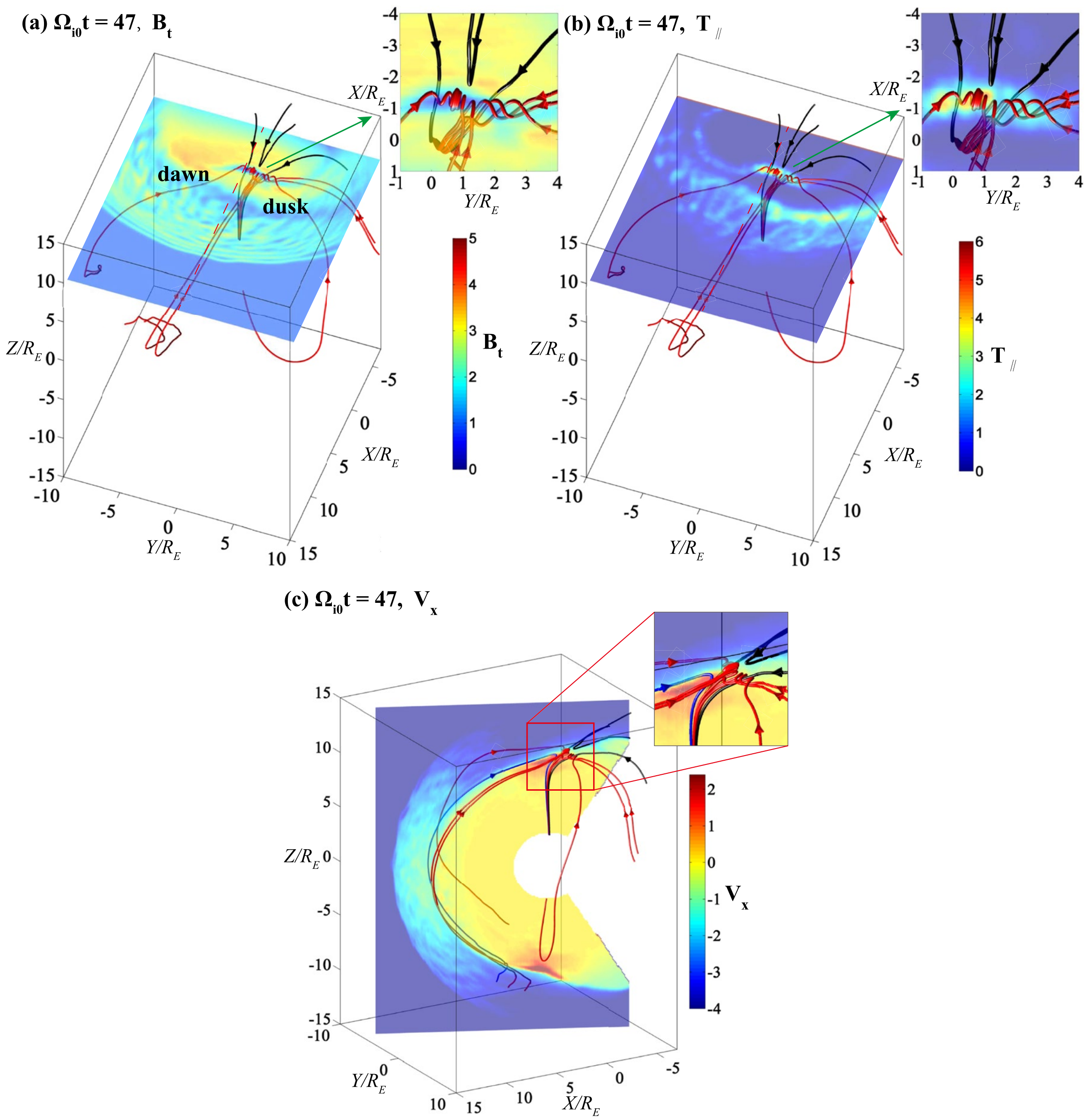

Figure 4. (a and b) The distribution of magnetic field magnitude B_t and parallel temperature $T_{\|}$ in $z = 10.6R_E$ plane obtained from Case 2 at $\Omega_{i0}t = 47$. The red dotted line represents the position of the noon-midnight meridian plane. (c) The distribution of ion velocity in x-direction (V_x) obtained from Case 2 at $\Omega_{i0}t = 47$. The plane is rotated for 15° around z-axis from the noon-midnight meridian plane. The red field lines represent the red flux rope; the black and blue field lines represent the reconnected magnetic fields. There is a zoom-in view of each figure.

no semi-open field lines (connected from magnetosphere to IMF, which only formed by the reconnection equatorward of the cusp) in this HLMFR.

In many previous studies, the high latitude magnetopause reconnection with the northward IMF was considered as single X line reconnection without flux ropes formed (Frey et al., 2019; Fuselier et al., 2014; Gosling et al., 1991; Song & Russell, 1992; Zong et al., 2005). Using a 3-D global MHD simulation, Berchem et al. (1995) determined the formation of HLMFRs only by examining the helical magnetic field lines. In our simulations, the HLMFRs with four topologies of magnetic field lines are formed with a decrease in the surrounding magnetic field magnitude, an increase in parallel temperature, and significant reconnection outflows. These characteristics provide more evidence to support the formation of HLMFRs under northward IMF. Our Simulations show that the high latitude reconnection occurs in the northern and southern

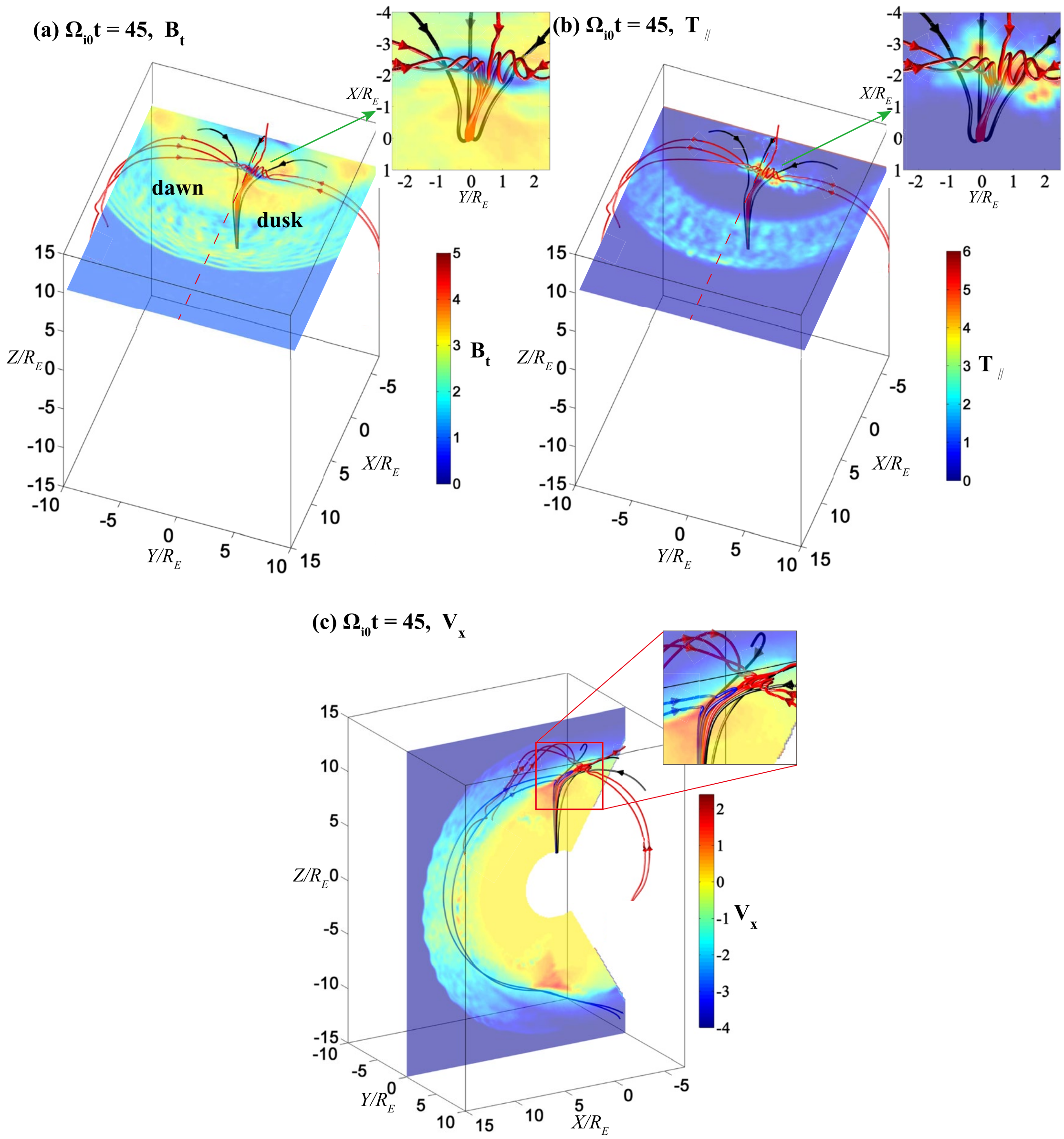

Figure 5. (a and b) The distribution of magnetic field magnitude B_t and parallel temperature $T_{\parallel}$ in $z = 10.6R_E$ plane obtained from Case 3 at $\Omega_{i0}t = 45$. The red dotted line represents the position of the noon-midnight meridian plane. (c and d) the distribution of ion velocity in x-direction (V_x) obtained from Case 3 at $\Omega_{i0}t = 45$. The plane is the noon-midnight meridian plane. The red field lines represent the red flux rope; the black and blue field lines represent the reconnected magnetic fields. There is a zoom-in view of each figure.

hemispheres, and this result is consistent with previous observations (Lockwood & Moen, 1999; Østgaard et al., 2005). Using a magnetosphere model, Fuselier et al. (2002) estimated that the length of high latitude reconnection X line during the northward IMF is about 3–5R_E, which is much shorter than that during the southward IMF (about 10–25R_E). Our simulations show that the scale of flux ropes is 2–3R_E long, which is similar to the scale of X lines obtained by Fuselier et al. (2002). Moreover, J. Guo et al. (2021a, 2021b) used a 3-D global hybrid simulation to show that when the IMF is southward, the number of flux ropes is 4–8, the length of flux ropes can be up to 12 R_E and the diameter of the flux ropes can be up to 2 R_E. However, in this study, we find that when the IMF is northward, the number of flux ropes is 1–2, the length of flux ropes is only about 3 R_E and the diameter of the flux ropes is less than 1 R_E. Therefore, the HLMFRs formed during the northward IMF are fewer and smaller than the flux ropes formed during the southward IMF.

High latitude magnetopause reconnection produces downward plasma outflows, resulting in the precipitation of energetic particles, which triggers auroras in the ionosphere (Øieroset et al., 1997). These auroras occur at postnoon (prenoon) with positive (negative) IMF B_y, in the northern hemisphere (Frey et al., 2003). Our simulations show the same results: in the northern hemisphere, the HLMFRs are on the dusk in Case 1 with an IMF clock of 80° (Figure 2), and the auroras triggered by these HLMFRs is also on the duskside; whereas, in Case 3, when the IMF clock angle is zero, the HLMFRs are near the noon-midnight meridian plane (Figure 5), and the auroras triggered by these HLMFRs also occurs at noon in the northern hemisphere. The reason for the dependence is that high latitude magnetopause reconnection prefers to occur at regions where the IMF is almost antiparallel to the geomagnetic field (e.g., Fuselier et al., 2002; Gosling et al., 1991; Laitinen et al., 2007; Lockwood & Moen, 1999; Luhmann et al., 1984; Phan et al., 2003). Since magnetic reconnection here is mostly antiparallel with a weak guide field, and a weak guide field leads to a weak core field (e.g., J. Guo et al., 2021a; Huang et al., 2012; Lu et al., 2020), therefore, the core field is not enhanced in the HLMFRs (see Figures 2f, 4a and 5a).

Steady high latitude magnetopause reconnection also leads to the generation of the ionospheric space hurricane during a several-hour period of northward IMF, and the dominant IMF B_y is an important factor that triggers the space hurricane (Zhang et al., 2021). Zhang et al. (2021) successfully revealed the formation mechanism of the space hurricane by performing a 3-D global MHD simulation. In Case 1, with a larger IMF B_y, the reconnection site is on the dusk side (see Figure 2), and the dawnward reconnection outflow can push the field lines (black field lines in Figure 2) moving dawnward. These results agree with the formation mechanism of the space hurricane, and the effect of HLMFRs on the formation of the space hurricane will be studied in the future by using the 3-D global hybrid simulation.

Data Availability Statement

In this study, the simulation results described in Section 3 are generated from our computer simulation model, and the simulation data used to plot the figures all can be downloaded from https://dx.doi.org/10.12176/01.99.00598.

Acknowledgments

This study was funded by the Strategic Priority Research Program of Chinese Academy of Sciences Grant no. XDB41000000, Key Research Program of Frontier Sciences CAS (QYZDJ-SSW-DQC010), and NSFC 41774169. The authors gratefully acknowledge the data resources from the "National Space Science Data Center, National Science & Technology Infrastructure of China."

References

Berchem, J., Fuselier, S., Petrinec, S., Frey, H. U., & Burch, J. L. (2003). Dayside proton aurora: Comparisons between Global MHD Simulations and IMAGE Observations. *Space Science Reviews*, *109*, 313–349. https://doi.org/10.1023/B:SPAC.0000007523.23002.92

Berchem, J., Joachim, R., & Maha, A. A. (1995). Magnetic flux ropes at the high-latitude magnetopause. *Geophysical Research Letter*, *22*, 1189–1192. https://doi.org/10.1029/95GL01014

Burton, R. K., McPherron, R. L., & Russell, C. T. (1975). An empirical relationship between interplanetary conditions and Dst. *Journal of Geophysical Research: Space Physics*, *80*(31), 4204–4214. https://doi.org/10.1029/JA080i031p04204

Dungey, J. W. (1961). Interplanetary magnetic field and the auroral zones. *Physical Review Letters*, *6*(2), 47–48. https://doi.org/10.1103/PhysRevLett.6.47

Frey, H. U., Han, D., Kataoka, R., Lessard, M. R., Milan, S. E., Nishimura, Y., et al. (2019). Dayside aurora. *Space Science Reviews*, *215*, 51. https://doi.org/10.1007/s11214-019-0617-7

Frey, H. U., Phan, T., Fuselier, S., & Mende, S. B. (2003). Continuous magnetic reconnection at Earth's magnetopause. *Nature*, *426*, 533–537. https://doi.org/10.1038/nature02084

Fuselier, S. A., Frey, H. U., Trattner, K. J., Mende, S. B., & Burch, J. L. (2002). Cusp aurora dependence on interplanetary magnetic field B_z. *Journal of Geophysical Research: Space Physics*, *107*(A7). https://doi.org/10.1029/2001JA900165

Fuselier, S. A., Petrinec, S. M., & Trattner, K. J. (2000). Stability of the high-latitude reconnection site for steady northward IMF. *Geophysical Research Letter*, *105*, 253–476. https://doi.org/10.1029/1999GL003706

Fuselier, S. A., Petrinec, S. M., Trattner, K. J., & Lavraud, B. (2014). Magnetic field topology for northward IMF reconnection: Ion observations. *Journal of Geophysical Research: Space Physics*, *119*, 9051–9071. https://doi.org/10.1002/2014JA020351

Gosling, J. T., Thomsen, M. F., Bame, S. J., Elphic, R. C., & Russell, C. T. (1991). Observations of reconnection of interplanetary and lobe magnetic field lines at the high-latitude magnetopause. *Journal of Geophysical Research*, *96*(A8), 14097–14106. https://doi.org/10.1029/91JA01139

Grandin, M., Turc, L., Battarbee, M., Ganse, U., Johlander, A., Pfau-Kempf, Y., et al. (2020). Hybrid-Vlasov simulation of auroral proton precipitation in the cusps: Comparison of northward and southward interplanetary magnetic field driving. *Journal of Space Weather and Space Climate*, *10*(1), 51. https://doi.org/10.1051/swsc/2020053

Guo, J., Lu, S., Lu, Q., Lin, Y., Wang, X., Huang, K., et al. (2021a). Structure and coalescence of magnetopause flux ropes and their dependence on IMF clock angle: Three-dimensional global hybrid simulations. *Journal of Geophysical Research: Space Physics*, *126*, e2020JA028670. https://doi.org/10.1029/2020JA028670

Guo, J., Lu, S., Lu, Q., Lin, Y., Wang, X., Huang, K., et al. (2021b). Re-reconnection processes of magnetopause flux ropes: Three-dimensional global hybrid simulations. *Journal of Geophysical Research: Space Physics*, *126*, e2021JA029388. https://doi.org/10.1029/2021JA029388

Guo, Z. F., Lin, Y., Wang, X., Vines, S. K., Lee, S. H., & Chen, Y. (2020). Magnetopause reconnection as influenced by the dipole tilt under southward IMF conditions: Hybrid simulation and MMS observation. *Journal of Geophysical Research: Space Physics*, *125*, e2020JA027795. https://doi.org/10.1029/2020JA027795

Hasegawa, H., Retinò, A., Vaivads, A., Khotyaintsev, Y., Nakamura, R., Takada, T., et al. (2008). Retreat and reformation of X-line during quasi-continuous tailward-of-the-cusp reconnection under northward IMF. *Geophysical Research Letters*, *35*, L15104. https://doi.org/10.1029/2008GL034767

Hasegawa, H., Wang, J., Dunlop, M. W., Pu, Z. Y., Zhang, Q.-H., Lavraud, B., et al. (2010). Evidence for a flux transfer event generated by multiple X-line reconnection at the magnetopause. *Geophysical Research Letters*, *37*, L16101. https://doi.org/10.1029/2010GL044219

Huang, C., Lu, Q. M., Zhang, H., Wu, M. Y., Dong, Q. L., Lu, S., & Wang, S. (2012). Kinetic simulations of the structure of magnetic island in multiple X line guide field reconnection. *Physics of Plasmas*, *19*(4), 042111. https://doi.org/10.1063/1.4704799

Laitinen, T. V., Palmroth, M., Pulkkinen, T. I., Janhunen, P., & Koskinen, H. E. J. (2007). Continuous reconnection line and pressure-dependent energy conversion on the magnetopause in a global MHD model. *Journal of Geophysical Research*, *112*, A11201. https://doi.org/10.1029/2007JA012352

Lavraud, B., Thomsen, M. F., Lefebvre, B., Schwartz, S. J., Seki, K., Phan, T. D., et al. (2006). Evidence for newly closed magnetosheath field lines at the dayside magnetopause under northward IMF. *Journal of Geophysical Research*, *111*, A05211. https://doi.org/10.1029/2005JA011266

Lee, L. C., & Fu, Z. F. (1985). A theory of magnetic flux transfer at the Earth's magnetopause. *Geophysical Research Letter*, *12*, 105–108. https://doi.org/10.1029/GL012i002p00105

Lee, L. C., Ma, Z. W., Fu, Z. F., & Otto, A. (1993). Topology of magnetic flux ropes and formation of fossil flux transfer events and boundary layer plasmas. *Journal of Geophysical Research*, *98*(A3), 3943–3951. https://doi.org/10.1029/92JA02203

Lin, Y., & Wang, X. Y. (2005). Three-dimensional global hybrid simulation of dayside dynamics associated with the quasi-parallel bow shock. *Journal of Geophysical Research*, *110*, A12216. https://doi.org/10.1029/2005JA011243

Lin, Y., & Wang, X. Y. (2006). Formation of dayside low-latitude boundary layer under northward interplanetary magnetic field. *Geophysical Research Letters*, *33*, L21104. https://doi.org/10.1029/2006GL027736

Lockwood, M., & Moen, J. (1999). Reconfiguration and closure of lobe flux by reconnection during northward IMF: Possible evidence for signatures in cusp/cleft auroral emissions. *Annales Geophysicae*, *17*, 996–1011. https://doi.org/10.1007/s00585-999-0996-2

Lu, S., Angelopoulos, V., Artemyev, A. V., Pritchett, P. L., Sun, W. J., & Slavin, J. A. (2020). Particle-in-cell simulations of secondary magnetic islands: Ion-scale flux ropes and plasmoids. *The Astrophysical Journal*, *900*, 145. https://doi.org/10.3847/1538-4357/abaa44

Luhmann, J. G., Walker, R. J., Russell, C. T., Crooker, N. U., Spreiter, J. R., & Stahara, S. S. (1984). Patterns of potential magnetic field merging sites on the dayside magnetopause. *Journal of Geophysical Research: Space Physics*, *89*(A3), 1739–1742. https://doi.org/10.1029/JA089iA03p01739

Øieroset, M., Phan, T. D., Haggerty, C., Shay, M. A., Eastwood, J. P., Gershman, D. J., et al. (2016). MMS observations of large guide field symmetric reconnection between colliding reconnection jets at the center of a magnetic flux rope at the magnetopause. *Geophysical Research Letter*, *43*, 5536–5544. https://doi.org/10.1002/2016GL069166

Øieroset, M., Sandholt, P. E., Denig, W. F., & Cowley, S. W. H. (1997). Northward interplanetary magnetic field cusp aurora and high-latitude magnetopause reconnection. *Journal of Geophysical Research*, *102*(A6), 11349–11362. https://doi.org/10.1029/97JA00559

Omidi, N., Blanco-Cano, X., Russell, C. T., & Karimabadi, H. (2004). Dipolar magnetospheres and their characterization as a function of magnetic moment. *Advances in Space Research*, *33*, 1996–2003. https://doi.org/10.1016/j.asr.2003.08.041

Onsager, T. G., Scudder, J. D., Lockwood, M., & Russell, C. T. (2001). Reconnection at the high-latitude magnetopause during northward interplanetary magnetic field conditions. *Journal of Geophysical Research*, *106*(A11), 25467–25488. https://doi.org/10.1029/2000JA000444

Østgaard, N., Mende, S. B., Frey, H. U., & Sigwarth, J. B. (2005). Simultaneous imaging of the reconnection spot in the opposite hemispheres during northward IMF. *Geophysical Research Letter*, *32*, L21104. https://doi.org/10.1029/2005GL024491

Phan, T., Frey, H. U., Frey, S., Peticolas, L., Fuselier, S., Carlson, C., et al. (2003). Simultaneous Cluster and IMAGE observations of cusp reconnection and auroral proton spot for northward IMF. *Geophysical Research Letter*, *30*, 1509. https://doi.org/10.1029/2003GL016885

Russell, C. T., & Elphic, R. C. (1978). Initial ISEE magnetometer results: Magnetopause observations. *Space Science Reviews*, *22*, 681–715. https://doi.org/10.1007/BF00212619

Shi, Q. Q., Zong, QG., Fu, S. Y., Dunlop, M. W., Pu, Z. Y., Parks, G. K., et al. (2013). Solar wind entry into the high-latitude terrestrial magnetosphere during geomagnetically quiet times. *Nature Communications*, *4*, 1466. https://doi.org/10.1038/ncomms2476

Song, P., & Russell, C. T. (1992). Model of the formation of the low-latitude boundary layer for strongly northward interplanetary magnetic field. *Journal of Geophysical Research: Space Physics*, *97*(A2), 1411–1420. https://doi.org/10.1029/91JA02377

Tan, B., Lin, Y., Perez, J. D., & Wang, X. Y. (2011). Global-scale hybrid simulation of dayside magnetic reconnection under southward IMF: Structure and evolution of reconnection. *Journal of Geophysical Research: Space Physics*, *116*, A02206. https://doi.org/10.1029/2010JA015580

Tóth, G., Chen, Y., Gombosi, T. I., Cassak, P., Markidis, S., & Peng, I. B. (2017). Scaling the ion inertial length and its implications for modeling reconnection in global simulations. *Journal of Geophysical Research: Space Physics*, *122*, 336–355. https://doi.org/10.1002/2017JA024189

Wang, S. M., Wang, R. S., Yao, S. T., Lu, Q. M., Russell, C. T., & Wang, S. (2019). Anisotropic electron distributions and whistler waves in a series of the flux transfer events at the magnetopause. *Journal of Geophysical Research: Space Physics*, *124*, 1753–1769. https://doi.org/10.1029/2018JA026417

Zhang, Q. H., Moen, J., Lockwood, M., McCrea, I., Zhang, B. C., McWilliams, K. A., et al. (2016). Polar cap patch transportation beyond the classic scenario. *Journal of Geophysical Research: Space Physics*, *121*, 9063–9074. https://doi.org/10.1002/2016JA022443

Zhang, Q. H., Zhang, Y. L., Wang, C., Oksavik, K., Lyons, L. R., Lockwood, M., et al. (2021). A space hurricane over the Earth's polar ionosphere. *Nature Communications*, *12*, 1207. https://doi.org/10.1038/s41467-021-21459-y

Zong, Q. G., Fritz, T. A., Spence, H., Frey, H. U., Mende, S. B., Korth, A., & Daly, P. W. (2005). Reverse convection and cusp proton aurora: Cluster, polar and image observation. *Advances in Space Research*, *36*(10), 1779–1784. https://doi.org/10.1016/j.asr.2004.09.023